Supporting Information

Gold Sunflower Microelectrode Arrays with Dendritic Nanostructures on the Lateral Surfaces for Anti-reflection and SERS

Sunil Mehla,[†] Ahmad Kandjani,[†] Victoria Coyle,[†] Christopher J. Harrison,[§] Mei Xian Low,[‡] Richard B. Kaner*,[⊥] Ylias Sabri*,[†] Suresh K. Bhargava*,[†]*

All correspondence to be addressed to suresh.bharagava@rmit.edu.au

Experimental Methods

Photolithography. A 200 nm conducting Ti nm film was deposited on Si wafers using e-Beam evaporation. The arrays were patterned on Ti coated Si wafers using image reversal lift-off patterning. The wafers were first cleaned with water, acetone, isopropyl alcohol and O_2 plasma. AZ5214-E resist was spin-coated on the wafers at 3000 rpm for 30 seconds followed by a soft bake at 90 ºC for 90 seconds. The resist coated wafers were exposed using MLA-150 with a pattern resolution around 1 µm and an exposure power of 25 J/cm^2 followed by a hard bake at 120 ºC for 120 seconds and UV flood exposure for 17 seconds. The obtained wafers were developed using 1:4 water/AZ400K solutions for 45 seconds and washed with water to obtain well developed honeycomb patterned resist film. The wafer was further metallized by e-Beam evaporation of 10 nm Ti and 200 nm Au. Post metallization patterns were lifted-off in acetone under sonication. After lift-off well-defined Au disc arrays were obtained which were further coated with a SiO_2 film of 50 nm thickness using e-beam evaporation to obtain SiO_2 capped Au disc arrays. A total of 35 patches (5 rows × 7 columns) of a fixed area of 200 × 200 µm^2 were designed within a single chip of size 16 × 8 mm. Each row consisted of 7 patches, each having the same pitch size which were used to collect uniformity data. As the pitch size of the

array increases from 2 μm to 6 μm in a fixed area of 200 × 200 μm^2, the total number of discs decrease from 1,116 to 418, respectively, as shown in **Figure S1**. For cyclic voltammetry, electrochemical surface area and X-ray diffraction studies, sensor chips were also fabricated with patterned area of 3.1 × 3.1 mm^2.

Lateral Electrodeposition. One-step electrodeposition using a potentiostat (CH Instruments, CHI 760C) was performed on SiO_2 capped Au disc arrays to obtain SMA with a conventional three-electrode system consisting of a graphite counter electrode and an Ag/AgCl (3.0 M KCl) reference electrode. The electrolyte contained an aqueous solution of desired concentration of $HAuCl_4$ (3.4/1.7/1.0/0.5/0.2 mM) as the gold source and 1.0 mM $Pb(CH_3COO)_2$ as the chemical templating agent. The gold dendrites were grown for different electrodeposition durations at a constant voltage of 0.05 V. The electrodeposited samples were washed with deionized water and dried under a nitrogen atmosphere. Cyclic voltammetry (CV) studies and electrochemical surface areas (ESA) measurements were performed in 1.0 M H_2SO_4 at a scan rate of 100 mVs^{-1}.

Optical Measurements. The evaluate of the plasmonic activity of the developed SMA was performed using CRAIC Apollo UV-VIS-NIR spectrophotometer. Eight-point calibration was performed before each measurement based on the transmission spectra of holmium oxide, didymium and erbium for wavelength calibration and absorbance spectra of five calibration standards for intensity calibration. Reflectance spectrum was collected in a region of 50 × 50 μm^2 from the central regions of the array from five different patches of the same pitch and morphology. The collected data was used to calculated mean reflectance intensities and relative standard deviation (RSD) for each data point. For Au-SiO_2 disc arrays RSD values up to 5.33% were observed highlighting the high quality of patterning uniformity of spectral response. For

optimum SMA of 2 μm pitch and hierarchical dendritic morphology RSD values up to 14.52% were observed owing to the random alignment of electrodeposited gold dendrites. FTIR spectroscopy was performed using the same methodology and data was collected using a Perkin-Elmer Spotlight 400 Imaging Microscope.

SERS Measurements. SERS experiments were conducted using a Perkin Elmer Raman Station 200F (785 nm laser, spot size of 50 μm) with an exposure time of 10 seconds and 3 acquisitions per data point, with no background correction. The SERS spectra were background corrected using an in-house developed wavelet transform/signal removal algorithm to obtain uniform Raman spectra.[57] All error bars (represented by standard error of the mean), standard deviation and variance in the figures related to Raman experiments were obtained from 7 different patches with the same morphology of SMA with each data point containing 3 acquisitions. SERS mapping analysis was performed by first focusing the laser at the center of the 200 × 200 μm^2 active patch area and then performing a linear sweep across a grid of 225 points (15 × 15) with each grid point separated by 20 μm.

Modelling. A 3D electric current model of the electrode array was constructed using COMSOL Multiphysics 5.3. The model consisted of two parallel plates placed 200 μm apart, with the lower plate patterned hexagonally with conductive discs 5 μm in diameter and 200 nm high, approximating patterns fabricated experimentally. Pitch between adjacent discs was varied in-line with the experimentally achieved structures from 2 – 6 μm in increments of 1 μm. Planar surfaces of the working electrode in the intermediate region between the discs were modelled as insulating, while the top planar and lateral surfaces of the circular microelectrodes in the array were modeled as conductors with an insulating layer atop the top planar surfaces. The remaining volume between electrodes was modelled as water in place of the electrolyte solution

and a bias of 1 V was applied between the two electrodes. Electric field and current density were closely aligned, as the medium exhibits real impedance and electrodeposition occurs at DC. As only the distribution of current flow in the model was of interest, the precise conductivity of each element and the electric potential between electrodes was largely irrelevant, as this influences only the magnitude of the current flow. The model was limited to a 6 × 6 array of discs at all pitches, with an additional 40 µm of bulk electrode and electrolyte modelled outside of the array. Minimizing the size of the model was necessary to enable computation in a timely manner, and the selected size provided homogeneous results from the center of the array (approximating a larger array), while still exhibiting fringe (edge) effects at the array boundary. Meshing was configured such that exposed lateral surfaces of discs would have a maximum distance between elements of 200 nm, to provide good resolution in the regions where growth was observed.

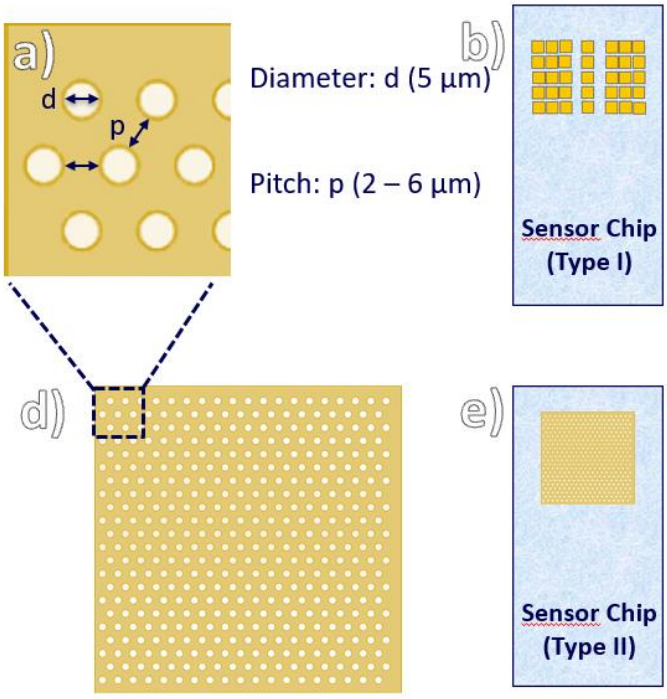

Sensor Chip (Type I)

c) Pitch	No. Of Discs
2	1,116
3	780
4	598
5	504
6	418

Sensor Chip (Type II)

f) Pitch	No. Of Discs
2	211,432
3	162,000
4	127,872
5	103,800
6	85,408

Figure S1. Design of SERS sensor chips used in this study. All designs for maskless photolithography were prepared using KLayout software; **a)** Zoomed-in image depicting disc

diameter ‘d’ and pitch ‘p’ of the array; **b)** Design of type I sensor chip consisting of 35 patches (5 rows × 7 columns) of 200 × 200 μm^2 area each. Each row consists of 7 patches of the same pitch and disc diameter; **c)** Exact number of discs in each patch of 200 × 200 μm^2 area. The number of discs decrease with increase in array pitch; **d)** Zoomed-out image of one patch consisting of hexagonally ordered disc arrays; **e)** Design of type II sensor chip with a patch area of 3.1 × 3.1 mm^2 developed for cyclic voltammetry, electrochemical surface area and X-ray diffraction studies; **f)** Exact number of discs in each patch of 3.1 × 3.1 mm^2 area.

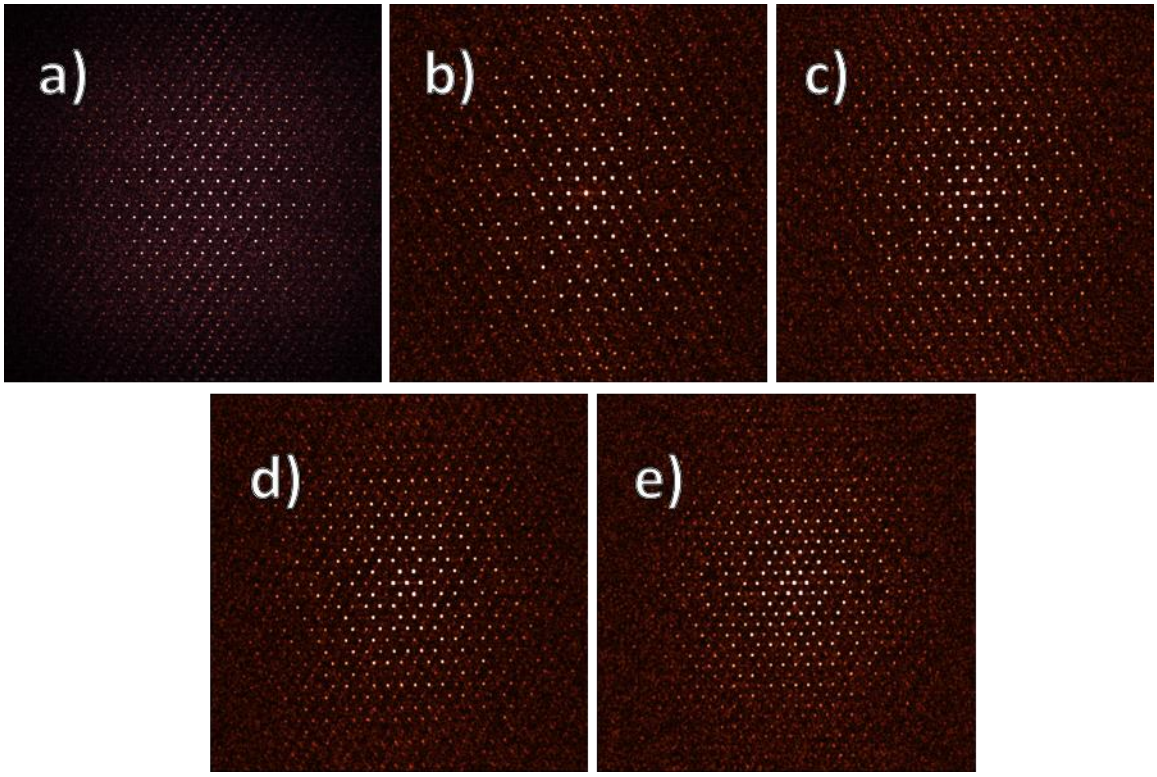

Figure S2. Fourier Transformed (FFT) images for low magnification SEM images of SiO_2 capped Au disc arrays depicting the presence of a long range and hexagonal order of arrangement and uniformity in structure for **a)** array pitch 2 µm; **b)** array pitch 3 µm; **c)** array pitch 4 µm; **d)** array pitch 5 µm, and; **e)** array pitch 6 µm.

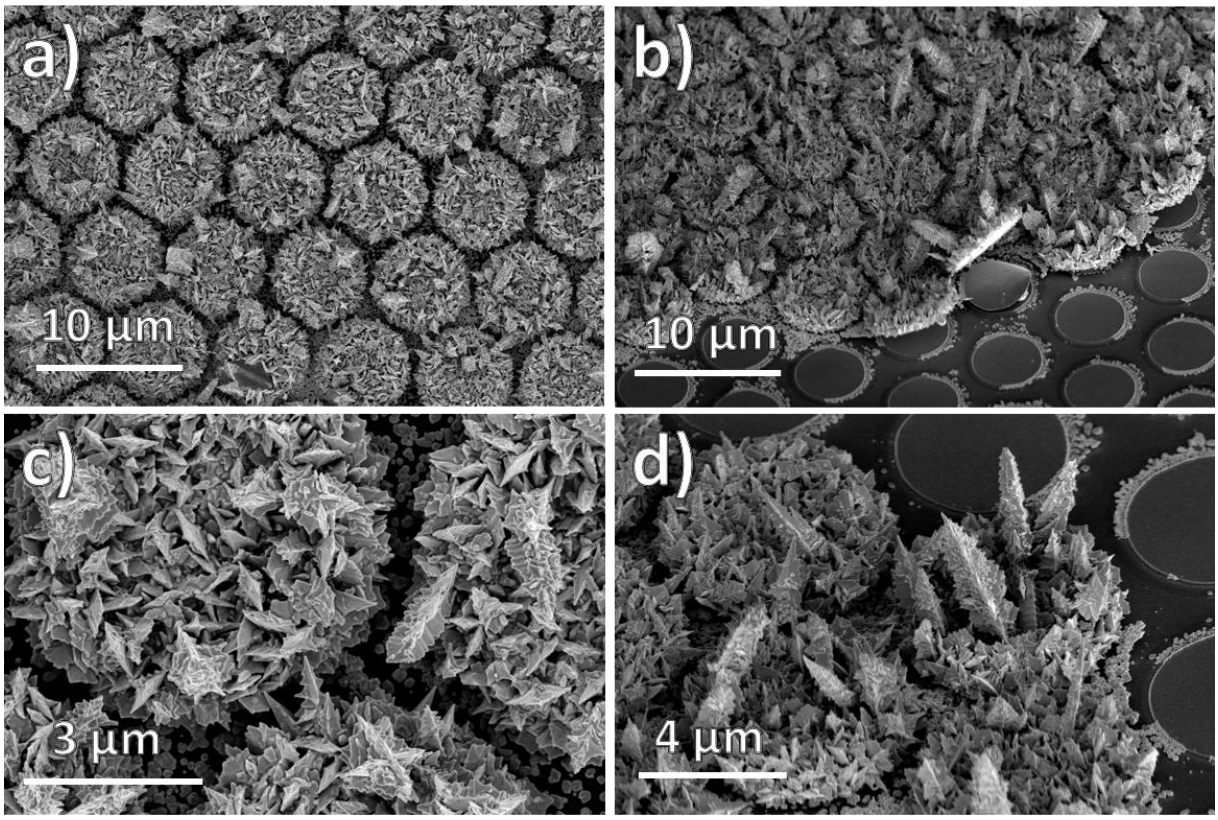

Figure S3. SEM images for electrodeposition of gold dendrites with 13.6 mM $HAuCl_4$ and 1.0 mM $Pb(CH_3COO)_2$ for 6 min on Au disc arrays without the insulating SiO_2 layer; **a)** Growth of large hierarchical dendrites on the top circular surfaces of Au disc arrays; **b)** Ripping of Au discs from the substrate surface due to the growth of large hierarchical dendrites; **c)** High magnification image of dendrites on top surfaces of Au disc; and **d)** Inclined SEM image of gold dendrites on disc arrays.

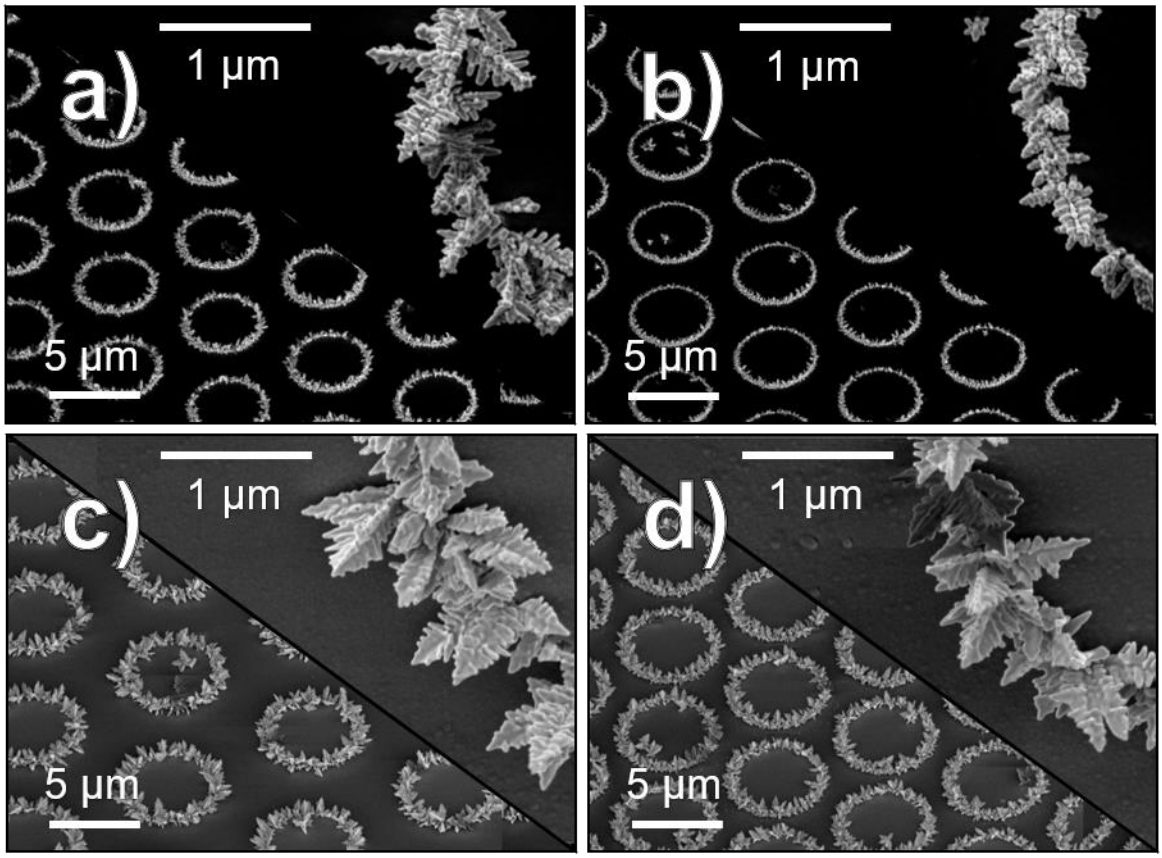

Figure S4. Dendrite morphology obtained for growth duration of 6 mins, array pitch of 4 µm and $HAuCl_4$ concentration of a) 0.5 mM; and b) 0.2 mM; dendrite morphology obtained for growth duration of 6 mins, $HAuCl_4$ concentration of 1.7 mM and array pitch of c) 5 µm; and d) 3 µm.

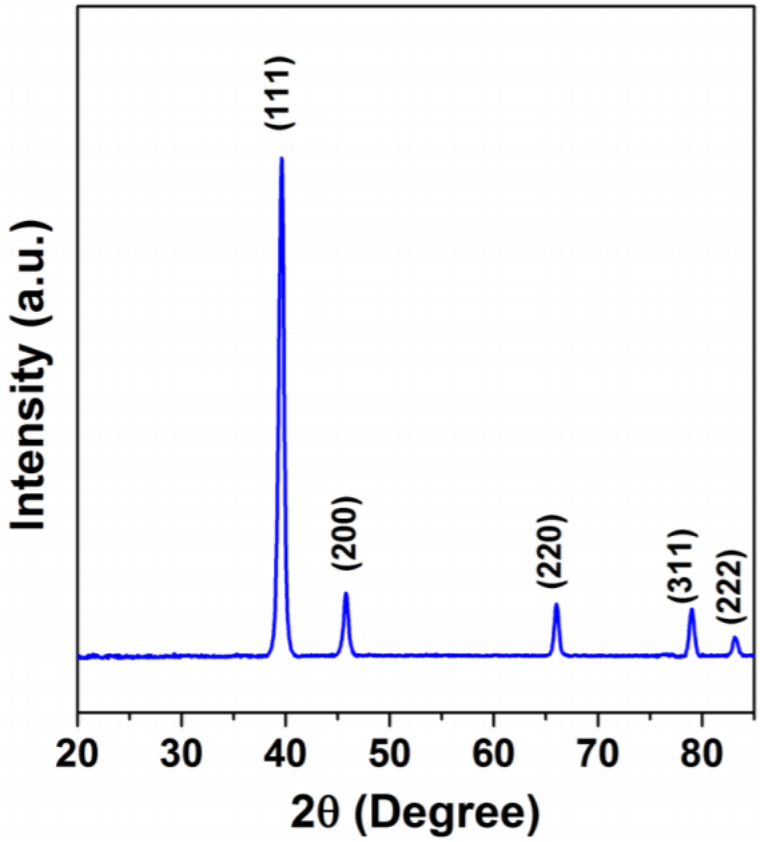

Figure S5. X-ray diffraction pattern for gold sunflower microelectrode arrays providing evidence for the existence of a high fraction of exposed (111) facets on deposited dendrites.

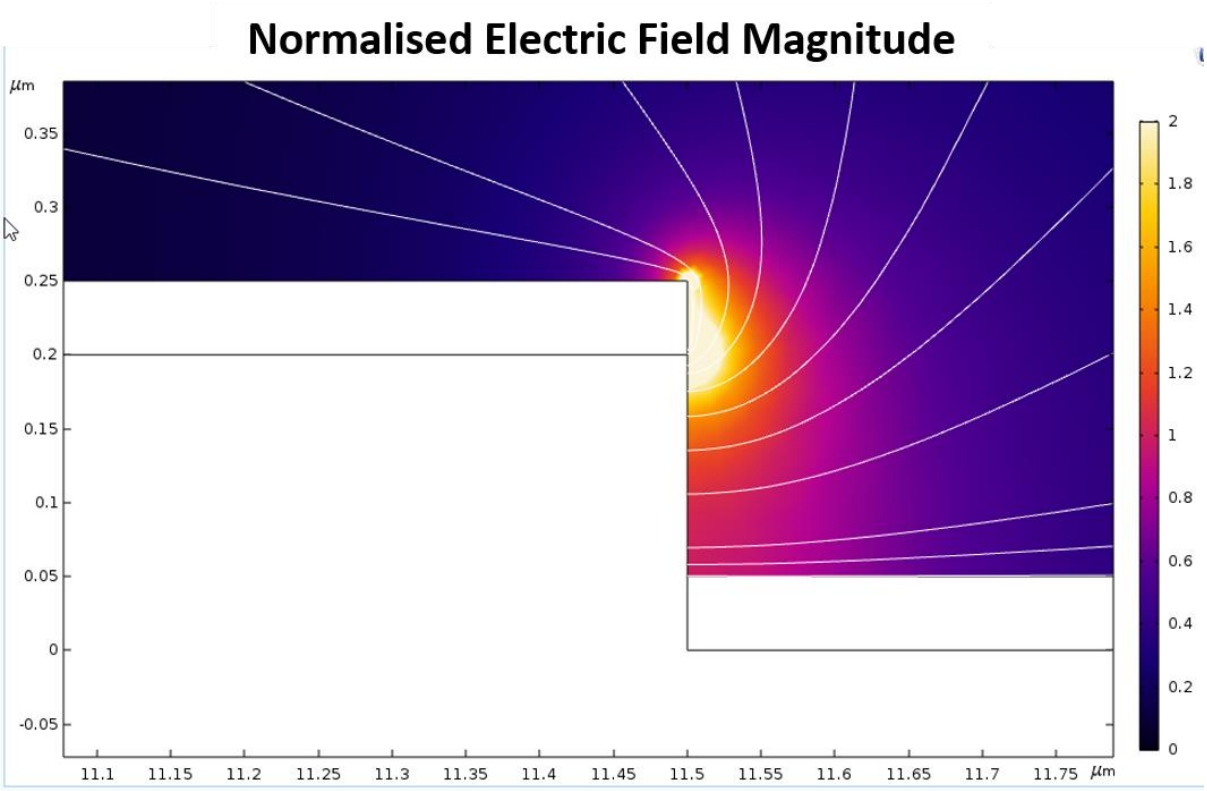

Figure S6. Normalized electric field magnitude and electric field lines obtained from FEM simulations at the lateral surface (fringe) of Au-SiO_2 discs. The growth of gold dendrites occurs along the electric field lines in a direction normal to the lateral surfaces and bend upwards towards the counter electrode.

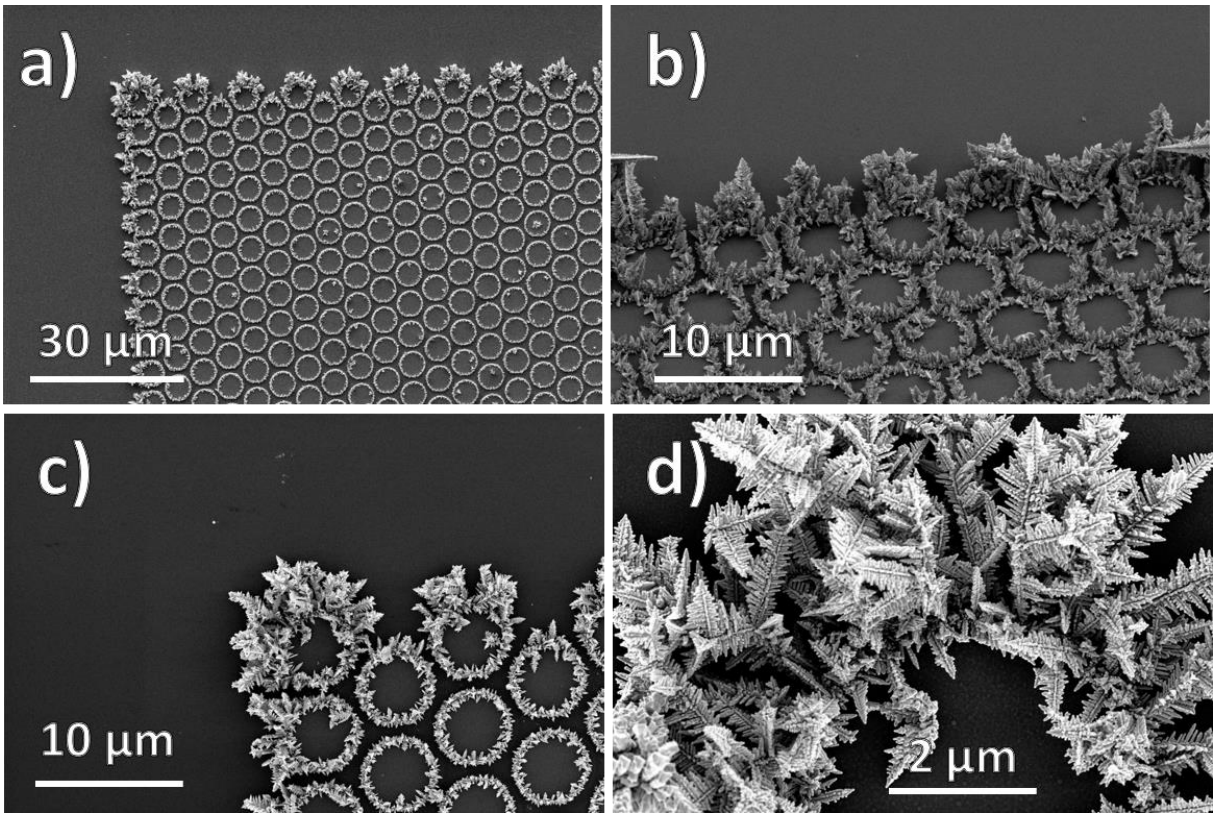

Figure S7. SEM images demonstrating higher growth at the edges of patterned areas of 200 × 200 µm^2 due to the fringe effect, showing both low and high magnifications; **a)** Low magnification SEM image of top left corner of patterned area; **b)** High magnification image of the top edge of the patterned area indicating asymmetric growth is restricted only to the first edge; **c)** High magnification SEM image of the top left corner of the patterned area; and **d)** Highly dendritic and hierarchical dendritic morphology of electrodeposited nanostructures as seen at high magnification.

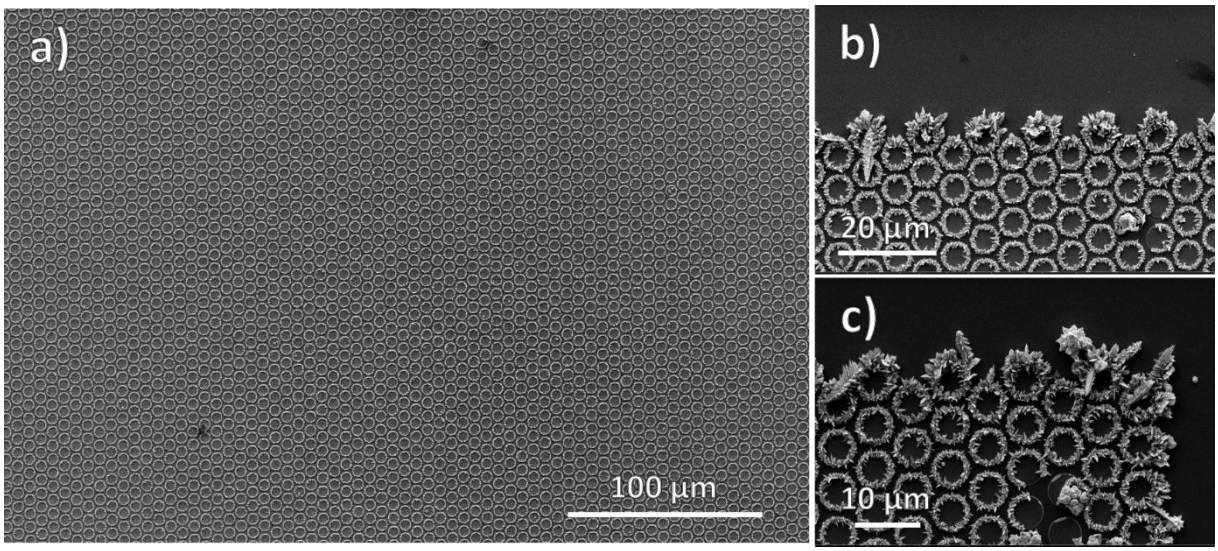

Figure S8. a) SEM image of long range and hexagonally ordered sunflower microelectrode arrays patterned over an area of size 3.1 × 3.1 mm^2; **b)** Asymmetric growth of hierarchical dendrites at the edge of the pattern; and **c)** Asymmetric growth of hierarchical dendrites at the corner of the patterned areas.

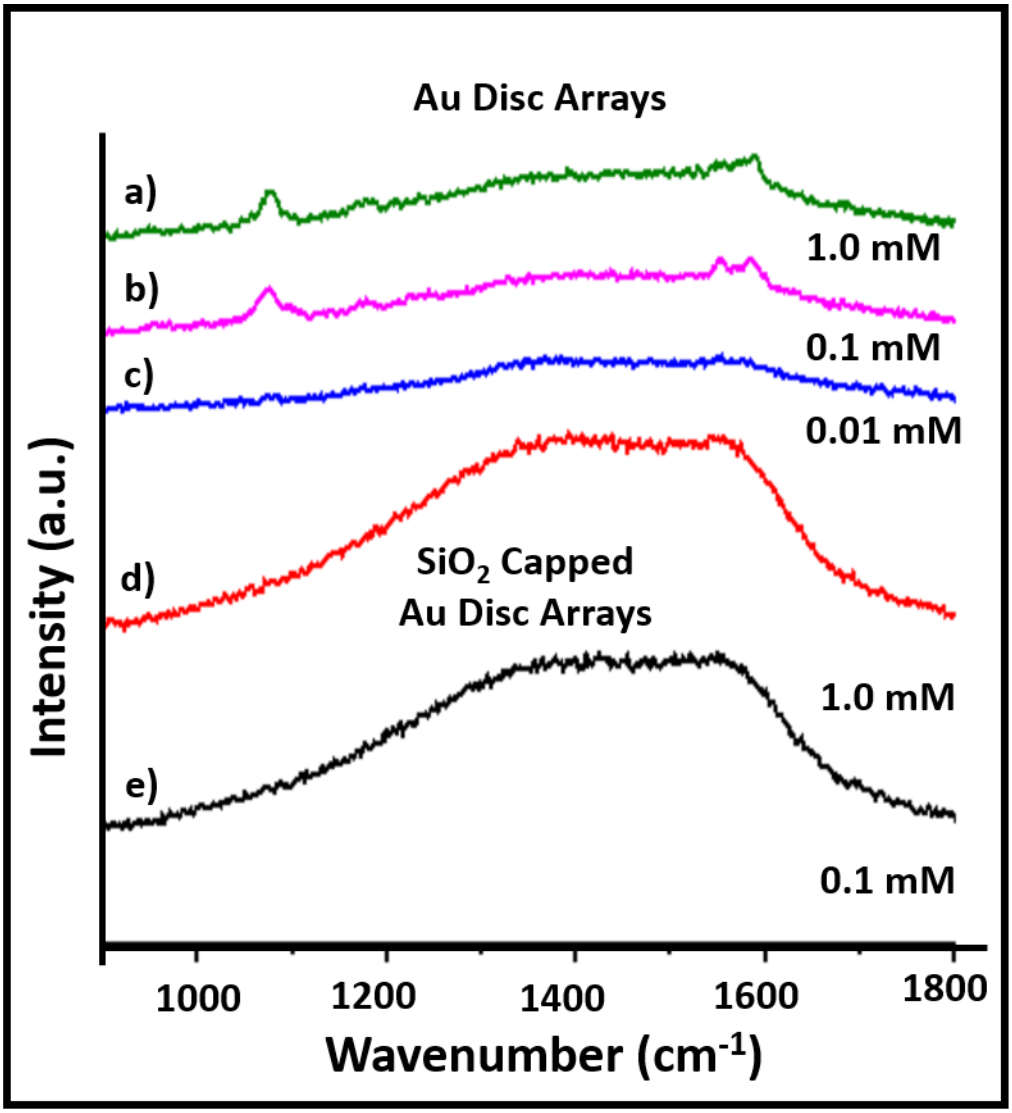

Figure S9. a) SERS spectra for Au disc array of pitch 2 µm and 1.0 mM ATP; **b)** SERS spectra for Au disc array of pitch 2 µm and 0.1 mM ATP; **c)** SERS spectra for SiO_2 capped Au disc array of pitch 2 µm and 0.01 mM ATP; **d)** SERS spectra for SiO_2 capped Au disc array of pitch 2 µm and 1.0 mM ATP; and, e) SERS spectra for SiO_2 capped Au disc array of pitch 2 µm and 0.1 mM ATP

4-ATP (powder)	4-ATP (Au-Sunflower)	Peak Shift Δ [cm^{-1}]	Assignments	Mode
1008 (w)	**1008 (w)**	**0**	**γCC + γCCC, 18a**	**a_1**
1085 (vs)	**1078 (vs)**	**-7**	**νCS, 7a**	**a_1**
1126 (w)	**1144 (w)**	**+18**	**δCH, 9b**	**b_2**
1179 (m)	**1180 (m)**	**+1**	**δCH, 9a**	**a_1**
1369 (w)	**1394 (w)**	**+25**	**νCC+δCH, 14b**	**b_2**
1425 (w)	**1442 (w)**	**+17**	**δCH +νCC, 3**	**b_2**
1493 (w)	**1484 (w)**	**-9**	**νCC+δCH, 19b**	**b_2**
1591 (s)	**1584 (vs)**	**-7**	**νCC, 8a**	**a_1**

Table S1. A comparison of Raman intensities, peak positions, Raman shifts and peak assignments for SERS spectra of sunflower microelectrode arrays with SERS spectra of ATP powder. The intensities were qualitatively treated and denoted as weak (w), medium (m), strong (s) and very strong (s). The vibration modes were denoted as stretching (ν) and bending (γ, δ).

$HAuCl_4$ conc. **Growth Duration**	**0.2 µM** **3 mins**	**0.5 µM** **3 mins**	**1.0 µM** **3 mins**	**1.7 µM** **3 mins**	**3.4 µM** **3 mins**	**1.7 µM** **1 mins**	**1.7 µM** **3 mins**	**1.7 µM** **6 mins**
Intensity of a_1 Peak (~1078 cm^{-1})	1490.33	2744.07	5185.55	7901.54	4927.72	4177.34	7901.54	17009.44
Intensity of b_2 Peak (~1144 cm^{-1})	131.92	150.63	247.13	1275.81	400.04	704.23	1275.81	6099.41
Intensity of b_2 Peak (~1442 cm^{-1})	191.19	387.78	560.70	937.81	576.47	1028.52	937.81	5093.31
Ratio b_2 (1144)/a_1 (1078)	0.09	0.05	0.05	0.16	0.08	0.17	0.16	0.36
Ratio b_2 (1442)/a_1 (1078)	0.13	0.14	0.11	0.12	0.12	0.25	0.12	0.30

Table S2. A comparison of intensities of the a_1 peak at 1078 cm^{-1} and the b_2 peaks at 1144 cm^{-1} and 1442 cm^{-1} and their ratios calculated from their SERS spectra for sunflower microelectrode arrays of varying morphologies and sizes when collected for a 1.0 µM ATP solution.

ATP concentration	**0.1 nM**	**1.0 nM**	**0.01 µM**	**0.1 µM**	**1.0 µM**	**0.01 mM**	**0.1 mM**	**1.0 mM**
Intensity of a_1 Peak (~1078 cm^{-1})	18908.82	19407.33	17907.13	17009.44	20780.94	20212.77	18615.80	1308.93
Intensity of b_2 Peak (~1144 cm^{-1})	5464.80	6391.51	5824.86	6099.41	7180.80	7005.61	5349.79	602.08
Intensity of b_2 Peak (~1442 cm^{-1})	4871.04	5650.66	4668.16	5093.31	4996.51	5207.48	3777.76	565.95
Ratio b_2 (1144)/a_1 (1078)	0.29	0.33	0.33	0.36	0.35	0.35	0.29	0.46
Ratio b_2 (1442)/a_1 (1078)	0.26	0.29	0.26	0.30	0.24	0.26	0.20	0.43

Table S3. A comparison of intensities of the a_1 peak at 1078 cm^{-1} and the b_2 peaks at 1144 cm^{-1} and 1442 cm^{-1} and their ratios calculated from their SERS spectra for sunflower microelectrode arrays of hierarchical dendritic morphology electrodeposited for a duration of 6 mins using 1.7 mM $HAuCl_4$ and an array pitch of 2 µm when collected for a variation in ATP concentration from 0.1 nM to 1.0 mM.

S. No.	Composition	Structure	Fabrication Methodology	Excitation Wavelength (nm)	Analyte	Limit of Detection	Relative Standard Deviation (%)	Ref.
1	Ag – Au	Ag nanoparticles on Au dendrites	Template-free electroreduction on patterned microelectrodes	785	Fentanyl	0.078 ppm	28.0 – 73.0	[1]
2	Au	Au film on SiO_2@Si pillars	Evaporated Au film on pillar arrays derived from laser interference lithography	633	Thionine acetate	8.7×10^{-6} M	23.95	[2]
3	Ag	Ag nanosheets on Cu foil	Template-free electrodeposition on Cu foil	532	4-amino thiophenol	10^{-8} M	20.0	[3]
4	Ag – Au	Ag film on Au nanoparticle clusters	Template-free electroreduction in colloidal lithography patterned nanobowl arrays	633	4-nitro benzene thiol	10^{-8} M	12.9%	[4]
5	Au Ag	Au rodlike aggregates Ag rodlike aggregates	Template-free electroreduction on colloidal lithography patterned hole arrays	633	Rhodamine 6G	10^{-11} M	12.0 (Au) 10.0 (Ag)	[5]
6	Ag	Ag on Au bowtie antennae	Template-free electroreduction on holographic lithography patterned microelectrodes	660	Benzene thiol	-	12.0	[6]
7	Ag	Randomly scattered Ag pyramids	Template-free electrodeposition in presence of PMMA spheres	532	Rhodamine 6G	10^{-9} M	7.3 – 8.7	[7]
8	Ag	Ag nanorod bundles	Templated electrodeposition in colloidal lithography patterned AAO templates	633	4-mercapto benzoic acid Methyl parathion	10^{-9} M (4-MBA) 21.5×10^{-9} (MP)	7.2%	[8]
9	Au	Au sunflower	Template-free electrodeposition on Au-SiO_2 disc arrays	785	4-amino thiophenol	5×10^{-10} M	**6.74** – 35.54	**This work**
10	Au	Au nanoflower	Template-free electroreduction on patterned microelectrodes	785	Crystal Violet Rhodamine 6G	10^{-10} M (CV) 10^{-11} M (R6G)	5.85 – 12.74	[9]

Table S4. Uniformity of SERS response recorded for hierarchical gold sunflower microelectrode arrays reported in this work in comparison with highly uniform SERS substrates reported in literature which were also fabricated using templated electrodeposition or template-free electrodeposition on patterned surfaces approaches.

References

1. Wilson, N. G.; Raveendran, J.; Docoslis, A., Portable identification of fentanyl analogues in drugs using surface-enhanced Raman scattering. *Sensors and Actuators B: Chemical* **2021,** *330*.
2. Kanipe, K. N.; Chidester, P. P.; Stucky, G. D.; Moskovits, M., Large Format Surface-Enhanced Raman Spectroscopy Substrate Optimized for Enhancement and Uniformity. *ACS Nano* **2016,** *10* (8), 7566-71.
3. Xia, Y.; Wu, Y.; Hang, T.; Chang, J.; Li, M., Electrodeposition of High Density Silver Nanosheets with Controllable Morphologies Served as Effective and Reproducible SERS Substrates. *Langmuir* **2016,** *32* (14), 3385-92.
4. Wang, Y.; Yu, Y.; Liu, Y.; Yang, S., Template-Confined Site-Specific Electrodeposition of Nanoparticle Cluster-in-Bowl Arrays as Surface Enhanced Raman Spectroscopy Substrates. *ACS Sens* **2018,** *3* (11), 2343-2350.
5. Wang, J.; Duan, G.; Liu, G.; Li, Y.; Xu, L.; Cai, W., Fabrication of gold and silver hierarchically micro/nanostructured arrays by localized electrocrystallization for application as SERS substrates. *Journal of Materials Chemistry C* **2015,** *3* (22), 5709-5714.
6. Yao, X.; Jiang, S.; Luo, S.; Liu, B. W.; Huang, T. X.; Hu, S.; Zhu, J.; Wang, X.; Ren, B., Uniform Periodic Bowtie SERS Substrate with Narrow Nanogaps Obtained by Monitored Pulsed Electrodeposition. *ACS Appl Mater Interfaces* **2020,** *12* (32), 36505-36512.
7. Chen, S.; Liu, B.; Zhang, X.; Mo, Y.; Chen, F.; Shi, H.; Zhang, W.; Hu, C.; Chen, J., Electrochemical fabrication of pyramid-shape silver microstructure as effective and reusable SERS substrate. *Electrochimica Acta* **2018,** *274*, 242-249.
8. Zhu, C.; Meng, G.; Zheng, P.; Huang, Q.; Li, Z.; Hu, X.; Wang, X.; Huang, Z.; Li, F.; Wu, N., A Hierarchically Ordered Array of Silver-Nanorod Bundles for Surface-Enhanced Raman Scattering Detection of Phenolic Pollutants. *Adv Mater* **2016,** *28* (24), 4871-6.
9. Zhang, L.; Hao, R.; Zhang, D.; You, H.; Dai, Y.; Liu, W.; Fang, J., Shape-Controlled Hierarchical Flowerlike Au Nanostructure Microarrays by Electrochemical Growth for Surface-Enhanced Raman Spectroscopy Application. *Anal Chem* **2020,** *92* (14), 9838-9846.